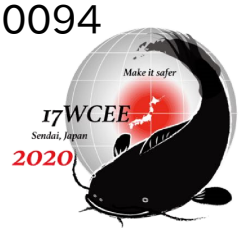

17th World Conference on Earthquake Engineering, 17WCEE
Sendai, Japan - September 13th to 18th 2020

Aftershock and microtremor array observations around the source area of the 2018 Hokkaido eastern Iburi earthquake: implications for generation mechanism of observed pulsive strong ground motions during the mainshock

M. Yoshimi[(1)], K. Iiyama[(2)], H. Morikawa[(3)], H Goto[(4)]

[(1)] *Senior research scientist, Geological Survey of Japan/AIST, yoshimi.m@aist.go.jp*
[(2)] *Researcher, Tokyo Institute of Technology, iiyama.k.aa@m.titech.ac.jp*
[(3)] *Professor, Tokyo Institute of Technology, morikawa.h.aa@m.titech.ac.jp*
[(4)] *Associate professor, Disaster Prevention Research Institute, Kyoto University, goto@catfish.dpri.kyoto-u.ac.jp*

Abstract

The 2018 Hokkaido eastern Iburi earthquake (Mw 6.6) is a crustal earthquake at 37 km depth ruptured a north-south strike east-dipping reverse fault. Strong ground motions were widely observed around the source area and in the Ishikari-Yufutsu sedimentary basin (IY basin), culminated with the maximum seismic intensity VII of the JMA scale at JMA Atsuma seismic station. Waveforms with clear velocity pulse having 1 to 3 dominant period were observed at seismic stations along the western vicinity of the source area: K-NET Mukawa (HKD126), JMA Atsuma (47004), KiK-net Atsuma (IBUH03), and Atsuma townhall (ATM), which commonly located along the basin edge of the IY basin. Velocity response spectra of these pulsive waveforms are comparable to that of the JR Takatori record during the 1995 Kobe earthquake, which has been used as design input for civil structures. Main purpose of our study is to reveal generation mechanism of these pulsive strong ground motions during the 2018 Iburi earthquake.

We conducted an aftershock observation and microtremor array surveys around the source area to investigate the spatial variation of the site amplification and subsurface velocity structure. 12 temporal seismic stations were deployed around the source area mainly along the western margin of the IY basin during 16th-21st Sep. 2018 to record around 20 aftershocks larger than magnitude two. Microtremor array survey with 3 component velocimeters was conducted at 10 locations with an array aperture of several meters to 1,000 meters to estimate velocity structures beneath the temporal stations and permanent stations as well. Site amplification is analyzed using S-wave records of the aftershocks. The H/H spectra, Fourier spectral ratio of the horizontal components of the S-wave of two sites, are calculated using a temporal station with flat H/V spectral ratio as a reference. Also velocity structures are inverted from the observed phase velocity data.

Nonlinear response at IBUH03 during the mainshock is analysed by simple linear response analysis to find the velocity reduction being needed for reproducing the observed waveforms and spectral ratio. Finally, we found that the nonlinear response is a plausible mechanism for the pulsive waveforms observed during the 2018 Iburi earthquake.

.

Keywords: subsurface velocity structure, H/H spectra, microtremor array survey, nonlinear response

1. Introduction

The 2018 Hokkaido eastern Iburi earthquake (Mw 6.6) is a crustal earthquake ruptured at 37 km depth in central Hokkaido, Japan, at 3:08 JST on September 6th, 2018. It caused huge number of landslides in the epicentral area on hills and slopes covered with volcanic pumice layers. It also gave arise the first ever power blackout on whole Hokkaido island, initiated from a shutdown of a thermal power plant located about 20 km from the epicenter. 43 people died in this earthquake: most of them were killed by the landslides and some by the carbon monoxide poisoning during the blackout. Building damage were, not severe as a whole, concentrated in the rural towns in the epicentral area; Mukawa town, Atsuma town, and Abira town.

Ground motions were felt all over the Hokkaido island. Observed ground motions were strong with the seismic intensity V+ or more in the JMA (Japanese Meteorological Agency) scale in the epicentral area and on the deep sedimentary basin (Ishikari-Yufutsu basin: IY basin) nearby. Especially at seismic stations in Mukawa, Atsuma, and Abira towns located in the west of the epicenter, observed ground motions were very strong with seismic intensity VI+ or VII (VII is the maximum and VI+ is the second maximum value in the JMA scale). They were as strong as those had been observed in the epicentral areas of shallow destructive earthquakes such as the 1995 Kobe (Mw 6.9) and the 2016 Kumamoto (Mw 7.0) earthquakes. It is very important to reveal why such strong ground motion was generated with an earthquake not shallow nor large like the 2018 Iburi earthquake.

Epicenter of this earthquake locates at the basin edge of the IY basin (Fig.1), which is recognized as active fault traces (red curves in Fig.1). Because the thick sediments existing beneath lowlands in the west of the basin edge (Yoshida et al. 2008), ground motion might have been amplified in the west of the epicenter. Takai et al. (2019) conducted aftershock observation and microtremor survey on a flatland of Mukawa town, where the seismic station HKD126 (K-NET Mukawa: NIED, 2019) that observed seismic intensity VI+ is located. They found the weak motion's predominant period to be shorter than the strong motion's dominant period of the 2018 Iburi earthquake and concluded that the nonlinear effect at HKD126 might be responsible to the potentially dangerous strong ground motion having dominant period of 1-2 seconds.

In this study, we focus on the site amplification of the epicentral area of the 2018 Iburi earthquake likewise Takai et al. (2019) did, but in wider area. We conducted an aftershock observation and a microtremor array survey around and between the seismic stations in Mukawa, Atsuma, and Abira town (Fig.1). Using results of the observations, generation mechanism of the observed strong ground motions during the mainshock are analyzed.

2. Near-field strong ground motion of the 2018 Hokkaido Eastern Iburi earthquake

Near-field strong ground motions observed at the west of the epicenter are shown in Fig.2: only the east-west component is shown here because this component is dominant among the horizontal observed motions presumably resulted by the reverse faulting on the north-south striking fault plane. Among them, waveforms with clear velocity pulse over 100 cm/s amplitude having dominant period 1 to 3 seconds are recognized for four stations: K-NET Mukawa (HKD126), JMA Atsuma (47004), KiK-net Atsuma (IBUH03), and Atsuma city hall (ATM), which commonly located in the west of the basin edge. Velocity response spectra of these pulsive waveforms are comparable to that of the JR Takatori record during the 1995 Kobe earthquake (Fig. 2), which has been used as a design input for civil structures in Japan. On the other hand, waveforms observed at north (HKD128, IBUH01) and east (not shown in the figure) of the source area were commonly dominated by shorter period waves, that were quite different from the waveforms observed in the western area. As the subsurface structure varies in this epicentral area, these clear differences of the observed ground motions might have resulted by the difference of the site amplification.

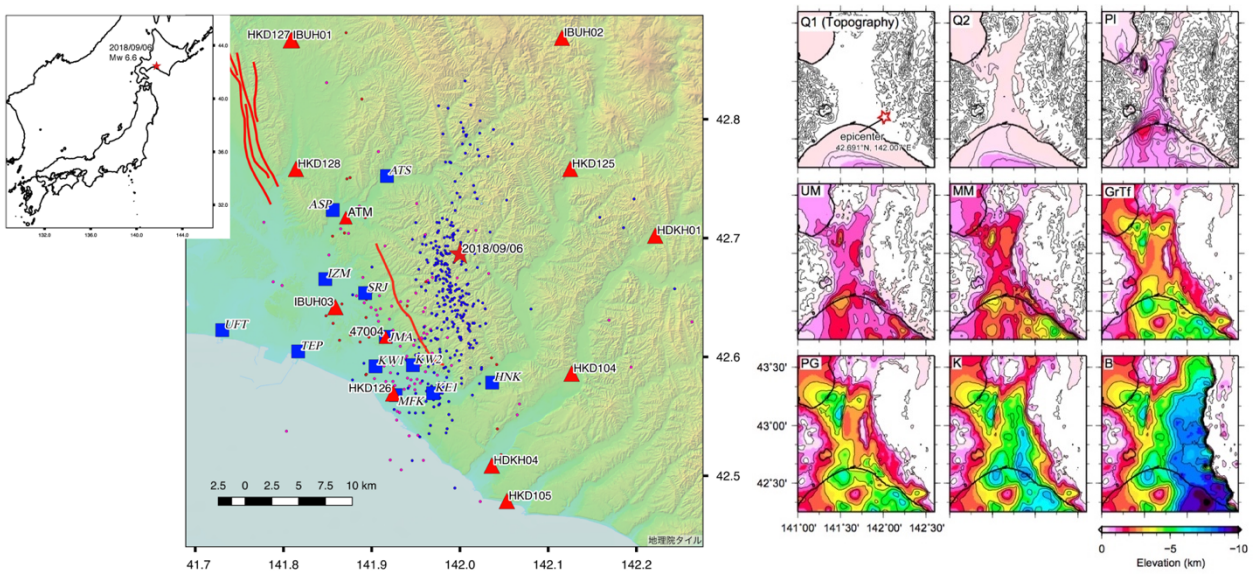

Fig.1 – Location of the aftershock observation and microtremor array survey (blue rectangle) and permanent seismic stations (red triangle) with epicenters of the main shock (red star) and aftershocks (dots) of the 2018 Hokkaido eastern Iburi earthquake. Red curves show active fault (right). Subsurface structure of the Ishikari-Yufutsu basin compiled by Geological Survey of Japan (Yoshida et al., 2008), showing epicentral area locates on the basin edge (left, UM corresponds to the upper depth of the Upper Miocene layer modeled as Vs=1.725 km/s).

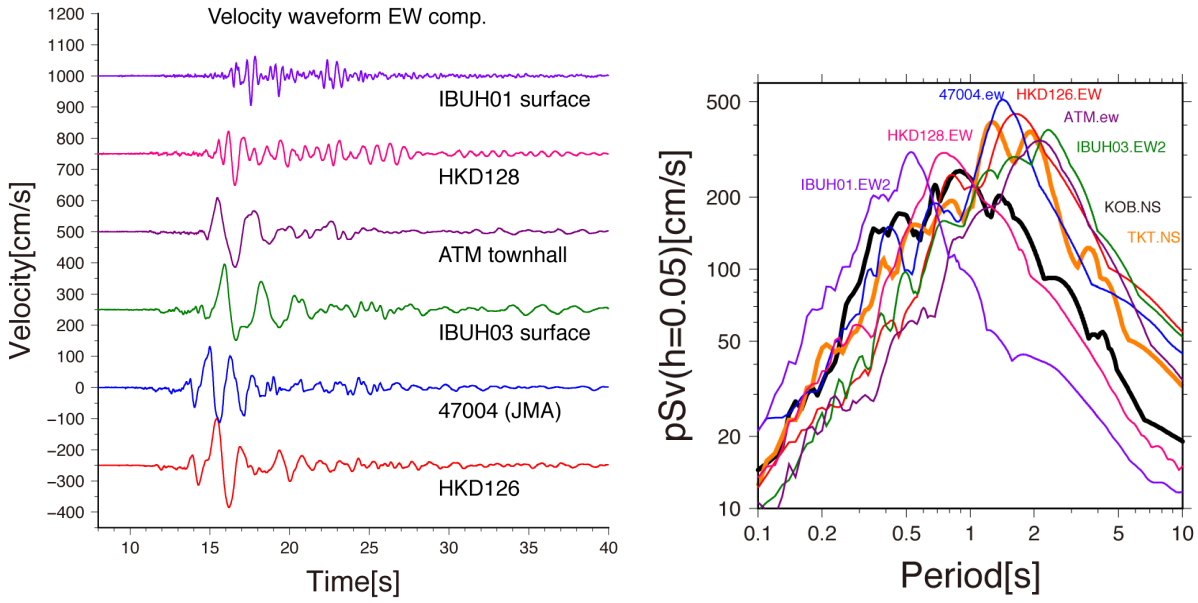

Fig.2 – Strong motion waveforms observed in the east of the epicentral area (left, integrated to the velocity waveform, see locations in Fig.1) and their pseudo velocity response spectra (right) compared with those of the 1995 Kobe earthquake (TKT: JR Takatori station, KOB: JMA Kobe).

3. Site observations

3.1 Aftershock observation

Aftershock observation was made for three to five days at twelve locations around the epicentral area (Fig.1, Table 1) one week after the mainshock of the Hokkaido eastern Iburi earthquake. Table 1 shows location, observed period, and type of the deployed seismometers of our temporal seismic stations. They all were installed on flatlands, still, ATS, ASP, and HNK stations were surrounded by the hills (Fig.1) composed of the Upper Miocene (Geological Survey of Japan, 2015). The site JMA is about 20 m from the seismometer at 47004, and the site MFK is about 300 m south-east of the HKD126. During our observation, 26 aftershocks larger than magnitude two (maximum event was M4.6) were detected by JMA. Though we used four types of seismometer having different noise level and sensitivity (Table 1), most of the aftershocks could be recognized in the data at every station.

For the purpose of analyzing site amplification, horizontal to horizontal spectral ratio (H/H spectra) of the S-wave between two sites is calculated using the aftershock records. Data by the SE321 velocimeters are used for the H/H spectra calculation because their signal to noise ratio (S/N ratio) are relatively high and more than half of the sites (seven sites: ATS, ASP, IZM, JMA, KW1, KE1, MFK) are covered if we use data by this seismometer. The site ATS is selected as a reference. The H/H spectra (Fig.3) is calculated using FFT of 40.96-second-long data after the onset of the S-wave. 13 events having high S/N ratio are selected for the calculation, whereas the number of events used for H/H spectra depends on the observation period of each site. The H/H spectra of the basin site, IZM, KW1, MFK, exhibit higher amplification with more than spectral ratio five in a frequency range between 0.5 to 2 Hz, compared with JMA and KE1. H/H spectra of the ASP is almost flat indicating slight amplification from ATS. These H/H spectra, as a whole, do not explain the observed predominant periods of the mainshock at 47004 and HKD126.

Table 1 – List of temporal seismic station for aftershock observation (Sensors: SE-321: Tokyo Sokushin's velocimeter 5V/kine T=10s, Titan: Nanometrics's balance triaxial accelerometer, JEP6A3: Mitsutoyo's high-damping moving coil-type accelerometer, GMR: aLab's giant magnetresistance sensor, Data logger: LS8800: Hakusan corp., AK002: aLab, ITK: aLab).

name	Lat.	Lon.	Start (yy/mm/dd hh:mm)	End (yy/mm/dd hh:mm)	Sensor and data logger	Landform
ATS	42.75802	141.92567	18/09/17 13:45	18/09/20 14:50	SE-321+LS8800	Hillside
ASP	42.73025	141.86316	18/09/17 13:00	18/09/20 15:43	GMR+ITK, SE-321+LS8800	Hillside
IZM	42.67231	141.85321	18/09/17 12:10	18/09/20 17:35	GMR+ITK, SE-321+LS8800	Flatland
SRJ	42.65984	141.89818	18/09/17 11:10	18/09/20 17:15	Titan+AK002	Flatland
JMA	42.62274	141.92068	18/09/16 18:00 18/09/17 10:49	18/09/21 11:53 18/09/21 11:53	GMR+ITK SE-321+LS8800	Flatland (47004)
UFT	42.63092	141.73496	18/09/16 15:30	18/09/21 14:45	GMR+ITK	Flatland
TEP	42.61182	141.82079	18/09/16 17:00	18/09/21 13:30	JEP6A3+AK002	reclaimed land (port)
KW1	42.59812	141.90846	18/09/17 17:30	18/09/21 12:20	GMR+ITK, SE-321+LS8800	Flatland
KW2	42.59842	141.95086	18/09/18 13:50	18/09/21 12:20	GMR+AK002	Flatland
KE1	42.57446	141.97316	18/09/17 09:15	18/09/21 11:15	SE-321+LS8800	Flatland
MFK	42.57356	141.93057	18/09/17 10:00	18/09/20 16:27	SE-321+LS8800	Flatland (300 m SE of HKD126)
HNK	42.582381	142.040515	18/09/17 09:30	18/09/21 10:45	TItan+AK002	Hillside

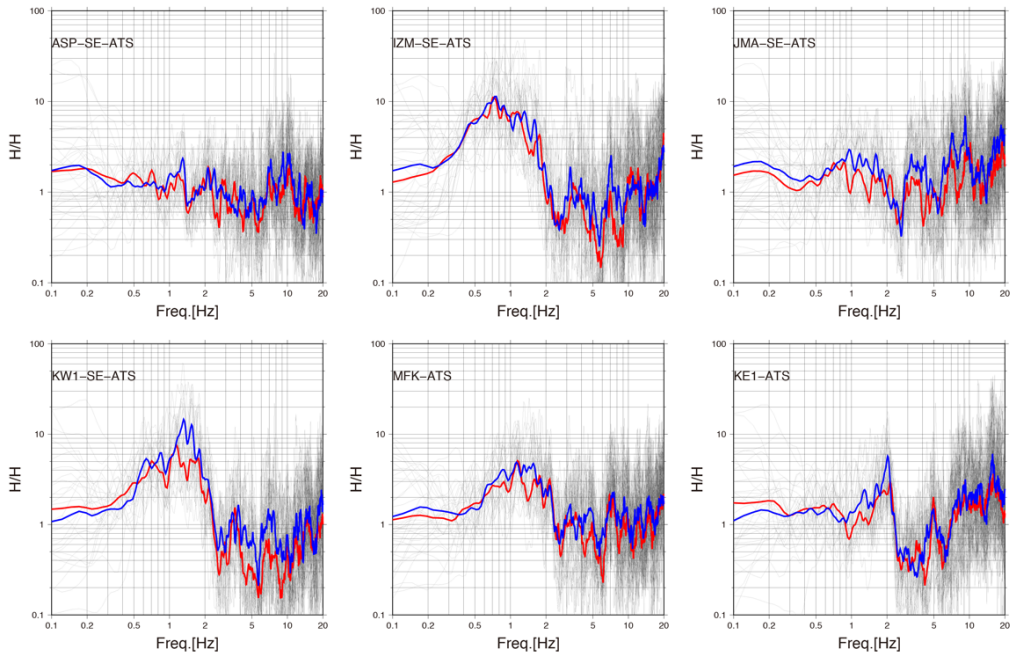

Fig. 3 – S-wave H/H spectra of the aftershocks of the temporal seismic stations deploying SE321+LS8800 system (ASP, IZM, JMA, KW1, MFK, and KE1 stations). Reference station is ATS. Averaged H/H spectra are drawn in red and blue.

3.2 Microtremor array survey

Microtremor array survey was conducted at 10 locations to estimate the subsurface velocity structure beneath the permanent seismic stations and our temporal stations listed in Table 2. Large aperture (radius up to 1,000 m) microtremor array observation were performed using four seismometers of SE-321 (5V/kine) or Lennartz LE-3D/5s (8V/kine) with LS-8800 data logger to make regular triangle array at each site. Vertical component of the observed microtremor data are analyzed with the SPAC method (e.g. Okada, 2003) using BIDO2.0 software (Tada et al., 2010) to obtain phase velocity of Rayleigh wave. By averaging phase velocities of every triangle array, unified phase velocity dispersion curve of the Rayleigh wave was obtained for each site. 1D S-wave velocity (Vs) structure of each array site was estimated from the observed phase velocity with the inversion technique using a GA method (Yamanaka and Ishida, 1996). In Fig.4, observed phase velocity and estimated 1D Vs structure are shown for the sites almost correspond to the Fig.3: array site ATM covers the permanent seismic station of Atsuma townhall in its aperture but is away from the temporally station ASP; MKW covers both HKD126 and MFK. Surface layer at every array site is quite soft, since the phase velocity in higher frequency range ($f > 5$ Hz) goes down to about 0.1 km/s.

Table 2 – Locations of microtremor array survey and its apertures.

Name	Lat.	Lon.	Apertures (array radius) [m]
ATM	42.72412	141.87787	R=1000, 500, 250, 125, 60, 30, 15, 5
IZM	42.666975	141.866400	R=1000, 500, 280, 50, 17.3, 3.5
SRJ	42.65907	141.89676	R=1000, 530, 200, 100, 27.7, 3.5
JMA	42.622389	141.920272	R=500, 180, 100, 28.3, 3.5

IBUH03	42.648170	141.867083	R=1000, 500
TEP	42.61051	141.82087	R=1000, 300, 60, 20, 3.5
KW1	42.59818	141.90862	R=1000, 500, 120, 50, 15, 3.5
MKW	42.578360	141.928702	R=1000, 500, 200, 100, 18.5, 3.5
KE1	42.582300	141.976745	R=1000, 500, 180, 60, 46, 11.5, 5, 1.7
HNK	42.582381	142.040515	R=1000, 300, 100, 16, 3.5, 1.7

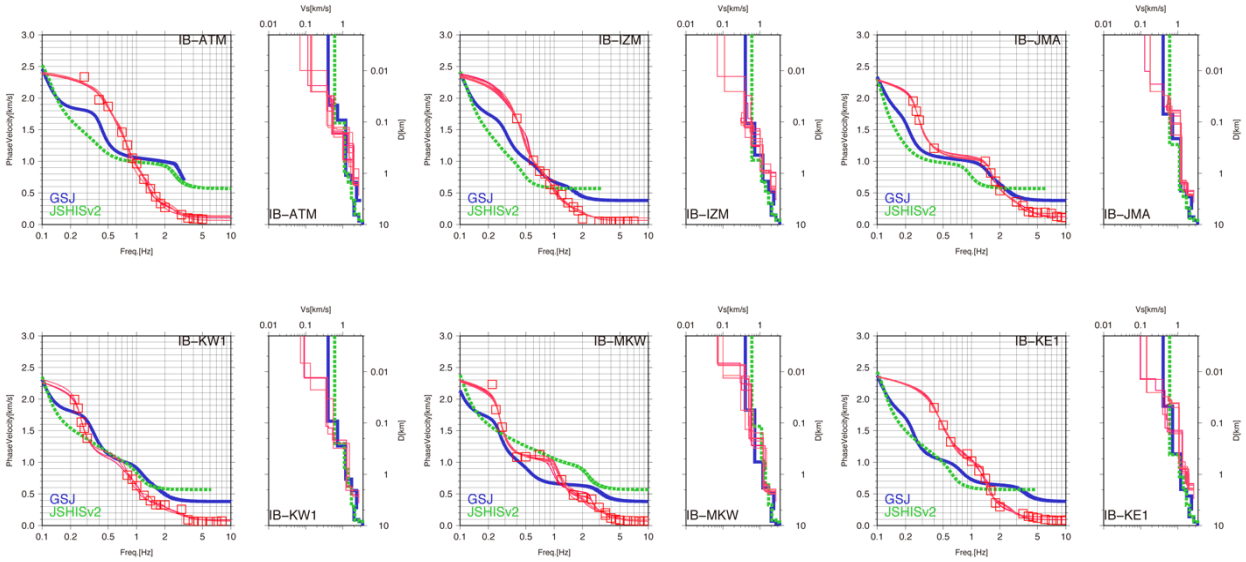

Fig. 4 - Observed phase velocity (red rectangle in the left panel in each plot) and estimated 1D S-wave velocity structures (right panel) at ATM, IZM, JMA, KW1, MKW, and KE1. Lines in blue and green, respectively, corresponds to the theoretical phase velocity and 1D Vs structure of the GSJ model (Yoshida et al., 2008) and J-SHIS v2 model (NIED, 2019). 1D velocity structures are drawn in log-log plot.

5. Discussions

5.1 Nonlinear response during the mainshock at IBUH03 seismic station

Site response obtained through our observation does not explain the dominant period of the pulsive velocity ground motion during the mainshock. Now, we consider nonlinear response during the mainshock. The KiK-net station IBUH03 consists of a pair of seismometers installed in a borehole (GL -153 m) and on the ground surface. Horizontal ground motions during the mainshock were successfully recorded with the seismometers of IBUH03. Fig. 5 in the left shows horizontal velocity waveforms at the borehole and at the ground surface of the IBUH03. Ground motions on the ground surface are clearly amplified by factor of more than five. In addition, timing of three distinct pulsive waves on the surface seen in the EW component between the time 15 to 23 sec. seem to be delayed from those of the borehole seen between 14 to 18 sec. indicating Vs reduction or nonlinear effect occurred. Spectral ratio of the surface waveform to the borehole waveform during the mainshock is much different from the spectral ratio of the weak motions (Fig.5 right). Peak frequency of the mainshock's spectral ratio shifts toward lower frequency compared with those of the weak motions. Thus, nonlinear response must be considered to explain the observed ground motion at IBUH03 during the 2018 Hokkaido eastern Iburi earthquake, so for the other sites.

To assess the nonlinearity during the mainshock, 1D linear seismic response analysis (Ohsaki, 1994) is conducted using the observed seismograms in the borehole of IBUH03 as the input motion. Measured Vs

structure of the IBUH03 published by NIED is employed as an initial model. Then, the Vs value and damping factor of each layer are searched with a trial and error basis to reproduce the spectral ratio and timing of the main pulses of the observed motion. Fig. 6 shows comparisons of the observation, initial model (linear model in blue), and Vs reduced model (pseudo nonlinear case, in red) of the ground motion (left) and the spectral ratio (middle). Initial and Vs reduced structures are shown in the right panel. We found that the spectral ratio and waveforms during the mainshock are well reproduced when the Vs values of the layers softer than Vs=500m/s are reduced by 50% and that of the shallowest layer by about 80%.

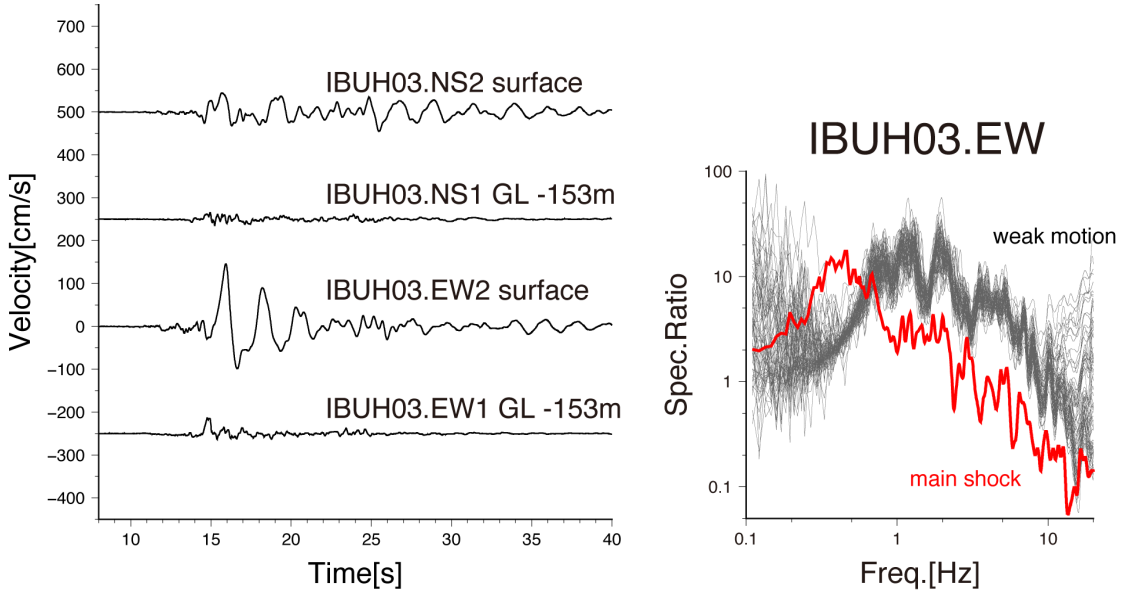

Fig. 5 – Observed ground motions at IBUH03 during the mainshock (left, time integrated to the velocity). Spectral ratio of the mainshock and weak motions between the borehole (GL -153 m) and the surface seismograph.

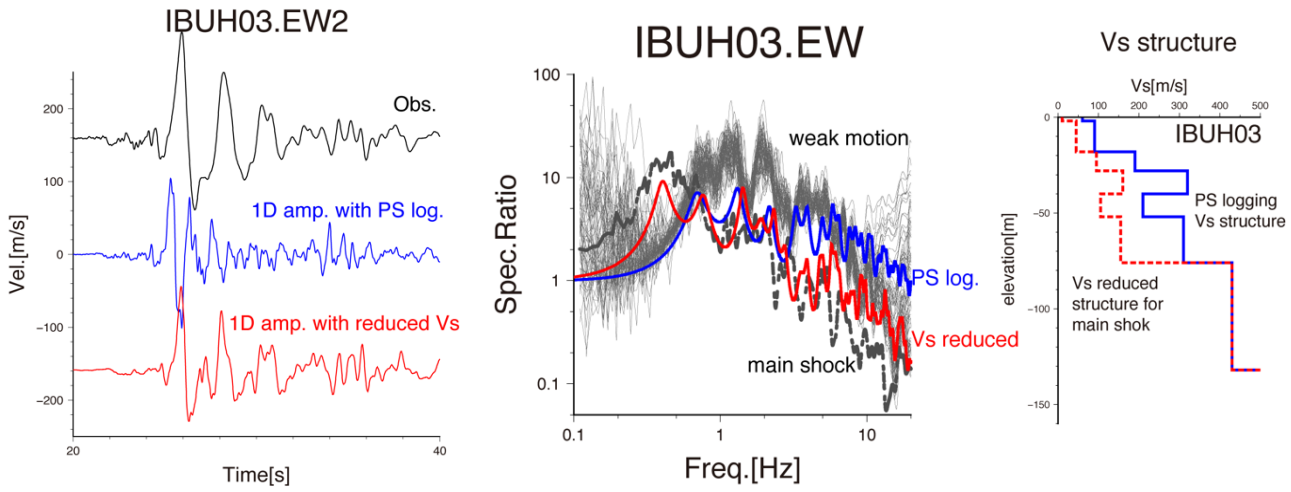

Fig. 6 – Comparison of observed and computed surface waveforms (left) and spectral ratios (middle) at IBUH03 by a 1D linear seismic response analysis using the borehole motion as an input assuming linear (in blue) and Vs-reduced (in red) 1D Vs structures (right). Observations are drawn in black or gray curves.

5.2 Reproduction of the pulsive waveforms considering velocity reduction

We finally calculate ground motions at HKD126, ATM townhall, and 47004 (JMA) during the mainshock. Since they are surface stations, no input motions were observed. As a rough trial, we assume the observed borehole motions at IBUH03 to be input ground motions for all sites. Inverted 1D Vs structures by our microtremor array survey are employed as the initial model for the site ATM and JMA, whereas published 1D Vs structure by Takai et al. (2019) is employed for the HKD126. The Vs values of the layers softer than Vs=500m/s are reduced to consider nonlinear effect during the mainshock. For simplicity, first guess of the reduction ratio is set to 50%, then the reduction ratio of the shallower layers is increased to fit the peak frequency of the observed spectral ratio. Fig 7 show the results. Observed waveforms and spectral ratios are nearly reproduced when the nonlinearity is considered, though further study is needed.

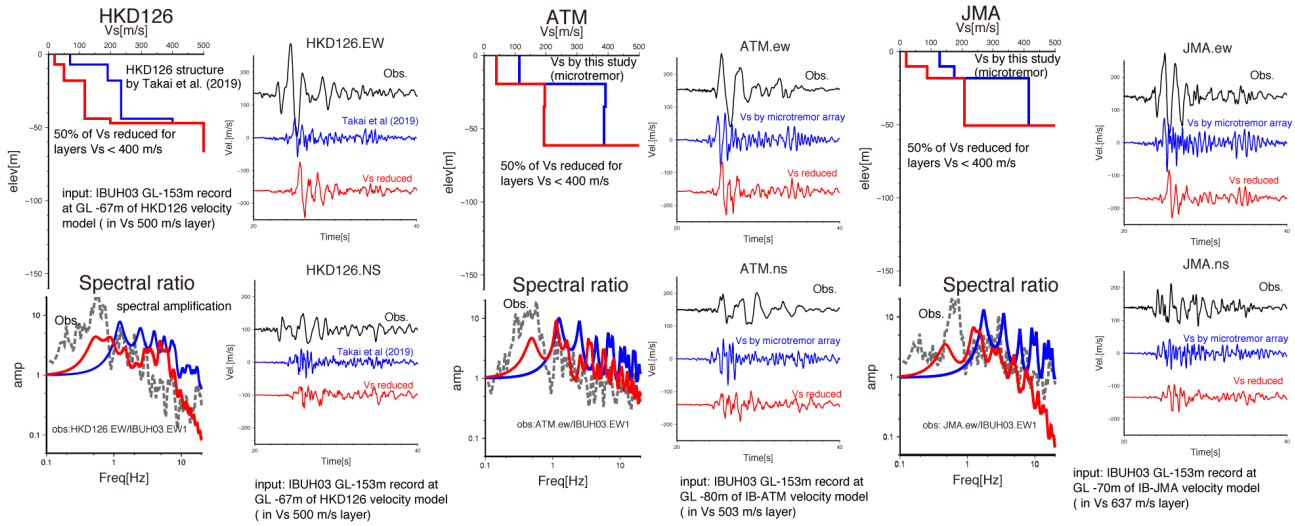

Fig. 7 – Comparisons of observed and computed waveforms (right panels) and spectral ratios (left bottom panel) during the mainshock at HKD126 (left), ATM townhall (middle) and 47004 (right) seismic stations. Waveforms and spectral ratio are computed by a 1D linear seismic response analysis using the borehole motion at IBUH03 as an input assuming linear (in blue) and Vs-reduced (in red) 1D Vs structures. Observations are drawn in black or gray curves. Observed spectral ratio is calculated using input wave (IBUH03 borehole) and observed wave at each station.

6. Conclusions

Generation mechanism has been analysed for the pulsive strong ground motions observed in the west of the epicentral area of the 2018 Hokkaido eastern Iburi earthquake. Aftershock observation and microtremor array survey were conducted in the epicentral area to obtain site amplification characteristics and Vs structures, which were thought to be responsible for the pulsive waves but not. Nonlinear response at IBUH03 during the mainshock is analysed by simple linear response analysis to find the velocity reduction being needed for reproducing the observed waveforms and spectral ratio. Finally, nonlinear response is a plausible mechanism for the pulsive waveforms observed at other seismic stations, ATM, HKD126, and 47004. Though it is obvious that further study is needed, for example on the input motions and velocity structures and nonlinear characteristics of soils, we believe that our results are quite important showing that the nonlinear response of soils plays an essential role in producing pulsive waveforms which are potentially hazardous.

Acknowledgement

This study was partially supported by JSPS KAKENHI Grant Numbers JP16H01842 and JP19H02406. Strong motion data of JR Takatori station is provided by the Railway Technical Research Institute. We used strong motion data provided by JMA, Hokkaido prefecture, and NIED. We thank Mr. Takeshi Sugiyama for providing part of the microtremor measurement data. We used program package DISPER80 (Saito, 1988) for calculations of surface wave phase velocities. Some of the figures are drawn using GMT package (Wessel et al., 2013).

References

[1] Takai N, Shigefuji M, Horita J, Nomoto S, Maeda T, Ichiyanagi M, Takahashi H, Yamanaka H, Chimoto K, Tsuno S, Korenaga M, Yamada N (2019): Cause of destructive strong ground motion within 1-2 s in Mukawa town during the 2018 Mw 6.6 Hokkaido eastern Iburi earthquake, Earth Planets and Space, 71:67.

[2] National Research Institute for Earth Science and Disaster Resilience (2019): NIED K-NET, KiK-net, National Research Institute for Earth Science and Disaster Resilience, doi:10.17598/NIED.0004

[3] Yoshida K, Yoshimi M, Suzuki H, Morino M, Takizawa F, Sekiguchi H, Horikawa H (2007): 3D velocity structure model of the Ishikari and Yufutsu sedimentary basins. Annual report on active fault and paleoearthquake research no. 7, pp 1–29

[4] National Research Institute for Earthquake Science and Disaster Resilience (2019): J-SHIS, National Research Institute for Earthquake Science and Disaster Resilience, https://doi.org/10.17598/nied.0010

[5] Geological Survey of Japan, AIST (ed.). (2015): Seamless digital geological map of Japan 1: 200,000., Geological Survey of Japan, National Institute of Advanced Industrial Science and Technology.

[6] Okada H (2003): The Micortremor Survey Method translated by Koya Suto), Geophysical Monograph Series, No.12, Society of Exploration Geophysics.

[7] Tada T, Cho I, Shinozaki Y (2010): New horizons in the utility of horizontal-motion microtremors, 7th International Conference on Urban Earthquake Engineering, (http://www.cuee.titech.ac.jp/Japanese/Publications/Doc/conference_7th.pdf)

[8] Yamanaka H, Ishida H (1996): Application of genetic algorithms to an inversion of surface-wave dispersion data, Bull. Seis. Soc. Am. 86, 436-444.

[9] Ohsaki Y (1994): Introduction to the Spectral Analysis of Earthquake Motion, Kajima publishing corp. 299 p.

[10] Saito M (1988): DISPER80: a subroutine package for the calculation of seismic normal-mode solutions, Seismological Algorithms-computational methods and computer programs, p. 469, ed. Doornbos DJ, Academic Press, New York.

[11] Wessel P, Smith WHF, Scharroo R, Luis JF, Wobbe F (2013): Generic Mapping Tools: Improved version released, EOS Trans. AGU, 94, 409-410.

